Korean J. Chem. Eng., **30**(3), 563-573 (2013)
DOI: 10.1007/s11814-012-0166-1

Computational fluid dynamics simulation of multiphase flow in packed sieve tray of distillation column

Sepideh Roshdi*, Norollah Kasiri*,†, Seyyed Hassan Hashemabadi, and Javad Ivakpour*****

*CAPE Center, School of Chemical Engineering, Iran University of Science & Technology, Narmak, Tehran 1684613114, Iran
**Computational Fluid Dynamics Research Laboratory, School of Chemical Engineering, Iran University of Science and Technology, Narmak, Tehran 1684613114, Iran
***Petroleum Refining Division, Research Institute of Petroleum Industry, Tehran 1485733111, Iran
(*Received 13 September 2012 • accepted 27 September 2012*)

Abstract−Computational fluid dynamic models (CFD) have been used for the description of hydraulic characteristics of packed sieve tray (PST). PST is a conventional sieve tray combined with a slice thickness of packing on the tray deck. Eulerian-Eulerian framework has been used to solve the equations of both liquid and gas phases assumed as two interpenetrating phases. A commercial scaled sieve tray has been simulated based on a three-dimensional unsteady state model. Comparison with experimental data proves good agreement for the simulation results under the studied conditions. Effects of the packing on the liquid velocity distribution, clear liquid height and vertical liquid volume fraction distribution have been investigated. The simulation results show that 3.08 cm of packing thickness could increase the clear liquid height up to 17 percent and froth height up to 10 percent as well as promoting froth density by 6 percent with the only drawback of increasing wet pressure drop up to 16 percent in froth regime.

Key words: Computational Fluid Dynamics (CFD), Sieve Tray, Packed Sieve Tray (PST), Clear Height, Froth Height, Wet Pressure Drop

INTRODUCTION

Sieve trays are one of the most widely used distillation column internals due to their simplicity in construction and low cost. But their lower efficiency among distillation column internals has led to much effort aimed to improve their hydraulic characteristics. Spagnolo and Chuang [1] were the first to investigate improving sieve tray efficiency through combining it with mesh packing. Their experimental work was performed in a column with 0.311 m diameter considering 25 mm thickness of a knitted mesh packing in a heavy water production process. Their results show that packing causes a reduction in the amount of entrainment up to 30% and 85% at low and high gas flow rates, respectively. Therefore, packing leads to a higher capacity and tray efficiency; however, the tray pressure drop will increase.

Chen et Al. [2], reported that a thin layer of packing on conventional sieve trays can be easily installed at low cost and could provide the best method for revamping of existing trays. They used a methanol-water system at a wide range of operating conditions in the column of 0.153 m diameter and 0.318 m tray spacing. Their findings showed that installation of packing (packing height was varied from 4.2 to 25.4 mm) increased the total pressure drop by 20% and visual froth height by about 10 to 20 percent. Chen et al. [3,4] studied the hydraulics of wire-mesh-PSTs for the separation of acetic-acid-water mixtures in a 0.150 mm diameter and packing thicknesses in the range from 0 to 30 mm column experimentally. Their experiments show that increasing froth height by about 10 to 20 percent could result in greater liquid holdup and improved capacity with lower entrainment and slightly greater pressure drop as a result of packing installation. They also reported similar results for air and water system at the hydraulic tests.

Salem [5] performed PST studies in a column of 0.078 m diameter and 85 cm height. The author found that cheaper Raschig ring packing causes an increasing of about 8% in tower efficiency compared to 36% increasing in tower efficiency for the more expensive wire pad of the same height.

Because of the costs, experimentation is not the optimum method to get detailed information about phase's treatment in distillation column. Currently published works demonstrate how CFD may be employed as an industrial design and research tool to study conventional sieve trays. Mehta et al. [6] modeled liquid phase flow on sieve geometry. Their model included comparison of x-velocity of water with the experimental work of Solari and Bell (1986) and residence time distributions (Mehta [7]). Effect of gas phase on the liquid phase behavior was studied with the addition of a source term in which vertical differences in gas velocity from hole to superficial velocity were considered. Fischer and Quarini [8] used a constant value of 0.44 for drag coefficient. Liu et al. [9] developed a two-dimensional liquid phase model with the source term considering the superficial gas velocity and the weir height. No changes in gas direction were assumed in the gas and liquid phase interaction term. Van Batten and Krishna [10] modeled sieve tray hydrodynamics to predict clear liquid height, dispersion density and clear liquid distribution in the flow path and vertical direction. They also predicted weir height effect on the clear liquid height with the application of a new drag coefficient based on the Bennett et al. [11] average liquid holdup fraction. Gesit et al. [12] performed excellent work to pre-

†To whom correspondence should be addressed.
E-mail: capepub@cape.iust.ac.ir

dict and validate the fluid flow pattern and hydraulic to demonstrate detailed information about gas and liquid phase velocity on the commercial scale sieve tray with drag coefficient based on the Bennett et al. [11] and Colwell [13] correlations. There are several studies that consider CFD modeling of the tray of distillation column [14-18].

The main objective of this work is to investigate the effect of inserting a slice thickness of packing on the conventional sieve tray to study the performance of tray in commercial scale. CFD simulations for packed beds cause difficulties because of the tiny mesh diameter and more computational time and complexity in packing structure [19]. Special drag forces and required sink terms were added to the modeling equations to make possible the simulation of packing on the tray. A transient two-phase flow model was developed to solve the equations in a three-dimensional state. Different drag force coefficients have been applied based on the average liquid holdup correlation for the packed zone [20], while Bennett's correlation has been used for the unpacked zone [11]. Sink terms have been considered for the gas and liquid momentum equations based on the well known Ergun equation [21]. Detailed hydraulic parameters of PST have been studied by the proposed model.

MODEL EQUATIONS

Eulerian multiphase model has been used to solve the equations. In this model the phases are considered as the interpenetrating continua. Equations in this approach are as follows:

Gas phase continuity equations:

$$\frac{\partial(\alpha_G\rho_G)}{\partial t}+\nabla\cdot(\alpha_G\rho_G U_G)=0 \tag{1}$$

Liquid phase continuity equations:

$$\frac{\partial(\alpha_L\rho_L)}{\partial t}+\nabla\cdot(\alpha_L\rho_L U_L)=0 \tag{2}$$

Gas phase momentum equation:

$$\frac{\partial(\alpha_G\rho_G U_G)}{\partial t}+\nabla\cdot(\alpha_G\rho_G U_G U_G)=\nabla\cdot(\alpha_G\mu_{G,eff}[\nabla U_G+(\nabla U_G)^T]) - \alpha_G\nabla P_G-M_{G,L}+\rho_G\alpha_G g+F_{GS} \tag{3}$$

Where $M_{G,L}$ is the interphase momentum transfer per unit volume between the phases. F_{GS} was added as momentum source term to Eq. (3) for modeling of porous media effects on the gas phase. Similarly, F_{LS} exists at the liquid momentum equation (Eq. (4)). These terms were calculated directly from the Ergun equation as described later.

Liquid phase momentum equation:

$$\frac{\partial(\alpha_L\rho_L U_L)}{\partial t}+\nabla\cdot(\alpha_L\rho_L U_L U_L)=\nabla\cdot(\alpha_L\mu_{L,eff}[\nabla U_L+(\nabla U_L)^T]) - \alpha_L\nabla P_L+M_{G,L}+\rho_L\alpha_L g+F_{LS} \tag{4}$$

Summation constrain for volume fractions:

$$\alpha_G+\alpha_L=1 \tag{5}$$

Gas and liquid phase volume fractions are linked to each other by Eq. (5).

Furthermore, pressure fields were assumed the same for both phases. Therefore, pressure is equal in the liquid and gas phases as follows:

$$P_G=P_L \tag{6}$$

Interphase momentum transfer should be supplemented to the set of equations for coupling the liquid and gas momentum as below.

$$M_{G,L}=\frac{3}{4}\rho_L\frac{\alpha_G}{d_G}C_d|U_G-U_L|(U_G-U_L) \tag{7}$$

The two phases are linked by Eqs. (6) and (7) as well.

Where d_G is bubble diameter. Drag coefficient can be evaluated from Eq. (8), which is a relation, presented for the rise of a swarm of large bubbles in the Churn-turbulent regime [10].

$$Cd=\frac{4}{3}\frac{\rho_L-\rho_G}{\rho_L}gd_G\frac{1}{V_{slip}^2} \tag{8}$$

Where,

$$V_{slip}=\frac{u_G}{\alpha_{G,Ave}}$$

V_{slip} is the slip velocity of the collection of the bubbles in relation to the liquid. $\alpha_{G,Ave}$ in Eq. (8) can be replaced from Bennett et al.'s correlation [11] (Eq. (9)) for average air gas volume fraction [10,12,15].

$$\alpha_{G,Ave}=1-\exp\left(-12.55\left(Vs\sqrt{\frac{\rho_G}{\rho_L-\rho_G}}\right)^{0.91}\right) \tag{9}$$

Where Vs, is the gas superficial velocity based on bubbling area.

In this work, to simulate the packed zone above sieve tray, additional source terms were added to both liquid and gas momentum equations based on the Ergun equation. These source terms (F_{GS} and F_{LS} in Eq. (3) and (4)) are not applicable in the unpacked zones. Source terms show both inertial and viscous solid phase resistances. Structured packing properties presented in Table 1 have been used to develop the sink terms as follows [21]:

$$F_{GS}=-\frac{\mu_{G,eff}}{\alpha}U_G-\frac{1}{2}C_2\rho_G U_G^2 \tag{10}$$

$$F_{LS}=-\frac{\mu_{L,eff}}{\alpha}U_L-\frac{1}{2}C_2\rho_L U_L^2 \tag{11}$$

Where;

$$\alpha=\left[\frac{d_{eq}^2\varepsilon_p^3}{150(1-\varepsilon_p)^2}\right];\ d_{eq}=\left[\frac{6(1-\varepsilon_p)}{a_p}\right]$$

Table 1. The model dimensions and packing properties

Tray diameter (m)	1.22
Tray spacing (m)	0.61
Outlet weir height (m)	0.05
Downcomer length (m)	0.572
Hole area over bubbling area (%)	5
Number of the holes	45
Hole diameter (m)	0.025
Downcomer area (%)	13
Void fraction	0.978
Packing specific surface area (m^2/m^3)	345
Packing thickness	0.0308

$$C_2=\left[\frac{3.5(1-\varepsilon_p)}{d_{eq}\varepsilon_p^3}\right];\ d_{eq}=\left[\frac{6(1-\varepsilon_p)}{a_p}\right]$$

C_2 and α refer to the inertial and viscous losses, respectively, and ε_p is the porosity of the packing and d_{eq} is equivalent diameter of packing.

Good estimation of gas/liquid interactions is required to attain more realistic results. Modifications of drag coefficient of liquid and gas phases in sieve trays have been done previously [8-10]. To study the gas/liquid interaction in the presence of the packing correctly, true estimation of drag coefficient (Eq. (8)) is required for the packed zone. V_{slip} in Eq. (8) is an unknown term for the packed zone which has not been investigated previously.

Average liquid volume fraction of froth, $(1-\alpha_{G,Ave})$ in Eq. (8), decreases in porous zone of sieve tray, because of the presence of packing. Therefore, its changes can be used in calculation of drag coefficient (Cd) and interphase momentum transfer term ($M_{G,L}$ (Eq. (7))). Therefore, $\alpha_{G,Ave}$ should be properly inserted in Eq. (8) for the packed zone. Average of liquid volume fraction in the packed zone ($\alpha^P_{L,Ave}$) can be estimated from the following correlation (Eq. (12)). Yin [20] used this correlation to predict average liquid volume fraction in packed distillation column. Yin et al. [22] also reported that increase of liquid hold-up with the liquid flow rate can be obtainable from the following equation at the packed distillation column.

$$\alpha^P_{L,Ave}=\frac{0.4184}{\varepsilon_p}\left(\frac{\mu_{L,eff}}{\rho_L}\right)^{1/6}(u_l a_P)^{0.5} \tag{12}$$

The mentioned correlation was used for the calculation of average liquid volume fraction in the packed section of PST. Eq. (12) is based on the ratio of volume fractions of gas and liquid phases, so solid phase volume fraction was not considered in it. The following equation was used to convert average gas volume fraction to a true value to be used in solving equations (taking into account the solid phase volume fraction).

$$\alpha_{G,Ave}{}^*=1-\frac{\alpha^P_{L,Ave}}{\varepsilon_p} \tag{13}$$

Eq. (8) can be used in this study for PST, by considering the similarity of hydrodynamic behavior in packed section of PST based on the reported experimental studies of PST [1-3]. Therefore, Eq. (8) can be used for PST by substituting average gas volume fraction from Eq. (13).

Turbulence equations could be coupled with previously presented equations by considering standard k-ε method with default coefficients implemented frequently for the liquid [10,12,14,16].

To validate wet pressure drop resulting from CFD modeling, a simple macroscopic momentum equation was considered based on the Lockett [23] formulations by replacing clear liquid height (h_l) from Bennett et al. [11] or Colwell correlations [13]. Wet pressure drop is calculated as follows.

$$P_1-P_2=V_s\rho_G(V_s-V_h)+\rho_L g h_l \tag{14}$$

Where, P_1 is the pressure on the bottom of tray, P_2 is pressure on the top of the froth region and V_h is the air hole velocity and V_s is the gas superficial velocity based on the bubbling area.

h_l (Clear liquid height) could be determined from Bennett [11] or Colwell correlations [13]. The set of the equations is given in

Table 2. Colwell ccorrelations (1981)

Colwell correlations (1981) for the calculation of clear liquid height and froth density

$h_l=\alpha_{L,ave}\left[h_w+\frac{0.49k}{C_b^{0.67}}\left(\frac{Q}{\alpha_{L,ave}W}\right)^{0.67}\right]$		15
$C_b=0.61+0.08\frac{h_{ow}}{h_w}$	$\frac{h_{ow}}{h_w}<=8.14$	16
$C_b=1.06+\left(1+\frac{h_{ow}}{h_w}\right)^{1.5}$	$\frac{h_{ow}}{h_w}>8.14$	17
$h_{ow}=\frac{h_l}{\alpha_{L,ave}}-h_w$		18
$\alpha_{L,ave}=\frac{1}{1+\eta}$		19
$\eta=12.6Fr'^{0.4}\left(\frac{AH}{AB}\right)^{-0.25}$		20
$Fr'=\frac{\rho_G V_s 2}{g h_l(\rho_L-\rho_G)}$		21

K at the Eq. (15) equals 1.49 (Lockett, 1968)

Table 3. Bennet et al. correlations (1983)

Bennet et al. correlations (1983) for the calculation of clear liquid height and froth density

$h_l=\alpha_{L,ave}\left[h_w+C\left(\frac{Q}{W\alpha_{L,ave}}\right)^{0.67}\right]$		22
$\alpha_{G,Ave}=1-\exp\left(-12.25\left(Vs\sqrt{\frac{\rho_G}{\rho_L-\rho_G}}\right)^{0.91}\right)$		23
$C=0.5+0.438\exp(-137.8h_w)$		24

Tables 2 and 3, Colwell correlation [13] for calculation of h_l, required trial and error procedure.

FLOW GEOMETRY AND BOUNDARY CONDITIONS

Geometry of studied sieve tray and its packing is shown in Figs. 1(a) and (b). Sieve tray dimensions are based on tray properties of Solari and Bell [24] experimental works shown in Table 1. In the current work, sieve tray and PST are kept the same in geometry with the only difference of addition of 3.08 cm of packing on the tray deck for PST (Fig. 1(b)). The properties of Gempack-Aw7 type of structure packing have been considered in the simulations [25]. Due to the symmetrical boundary at the tray center, only one-half of the tray can be simulated to decrease the computational time.

Liquid and gas velocities have been considered as inlet boundary conditions assuming that gas and liquid volume fractions at their inlet area are equal to 1 (Fig. 1(a)). Liquid velocity of water phase was varied from flat profile (Eq. (29)) to parabolic profile (Eq. (230)) at the high flow parameters [12]. They have been given in Table 4. Gas velocity inlet equation (Vhole) is given in Table 4 (Eq. (28)). It was calculated from Eqs. (25), (26), (27) and (28). A_b Percentage was considered as 0.76 over total area at the tray with 1.22 m diameter from ref. 24. Hole area percentage value, (φ), is 5 percent over bubbling area in the geometry of Solari and Bell. Its value (A_{hole}) was calculated from Eq. (25) in the Table 4. n Value (number of the holes on the tray) was considered 90 and hole diameter was cal-

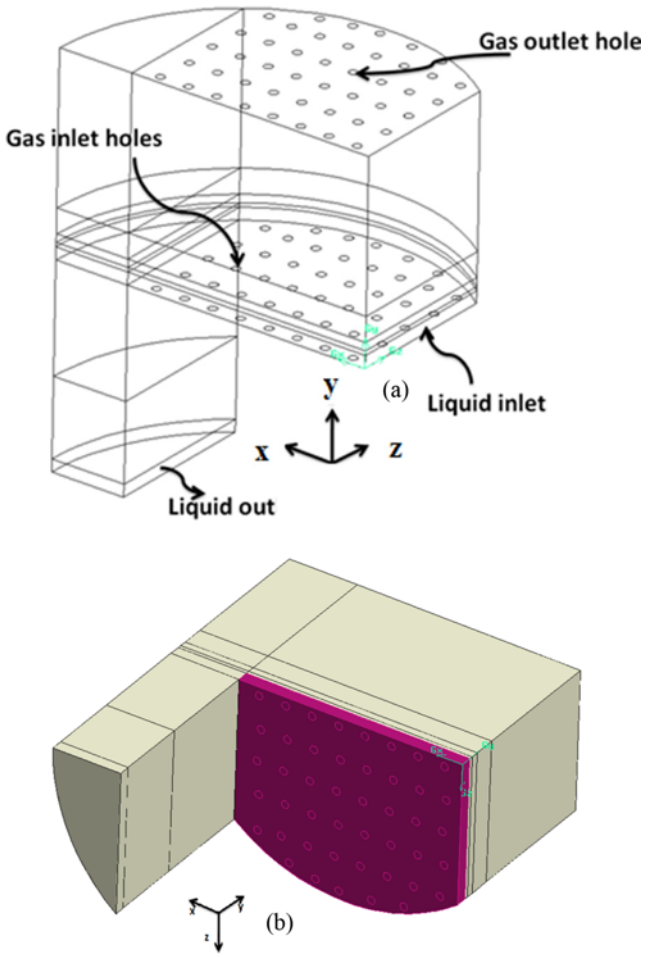

Fig. 1. Schematic diagram of (a): Sieve tray with boundary positions (b): Packed sieve tray.

Table 4. Boundary condition equations for gas and liquid phases

Boundary condition equations for the gas phase	
$A_{hole}=\varphi A_b$	25
$A_{hole}=n\pi\frac{d_{hole}^2}{4}$	26
$F_S=V_s\sqrt{\rho_G}$	27
$V_h=\frac{V_s A_b}{\left(\frac{n\pi d_{hole}^2}{4}\right)}$	28
Boundary condition equations for the liquid phase	
$u_l=\frac{Q}{h_{ap}W}$ 29 or $u_l=\frac{Q}{h_{ap}W}\left(1-\left(\frac{2z}{W}\right)^2\right)$	30
$k_{inl}=c_{pl}(u_l)^2$	31
$\varepsilon_{inl}=\frac{k_{inl}^{1.5}}{c_{pl}*u_l}$	32

c_{pl} * Was considered 0.002 for our problem

culated. Gesit et al. [12], reported that this number of holes gives good results with less computational time. The calculated Vhole value has been set as the velocity boundary condition at the inlet and outlet holes for the gas phase (Fig. 1(a)), assuming that only gas phase enters and leaves the inlet and outlet holes [12,15]. In the same way, u_l in Eqs. (29) and (30), was considered as liquid velocity boundary for outlet and inlet boundary condition for the liquid phase in Fig. 1(a) assuming that only liquid phase enters and exits from liquid inlet and outlet boundary (Fig. 1(a)). Turbulence values for the liquid inlet and outlet have been considered based on Eq. (31) and Eq. (32) in Table 4.

SOLUTION METHOD

Better initial estimations result in a more rapid convergence, so

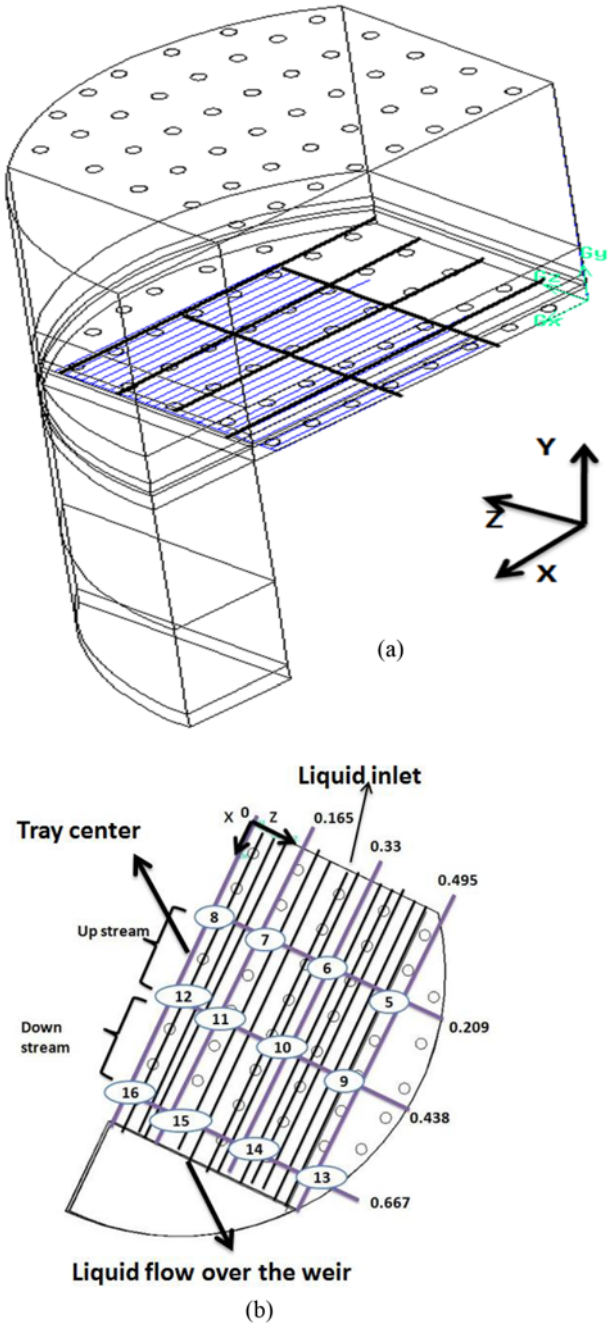

Fig. 2. Schematic diagram of probe positions and velocity lines in (a): 3D geometry of sieve tray (b): 2D geometry of sieve tray [6].

the calculation domain is subdivided into different zones to define true initial conditions at the different zones inside of a tray. True values for air and water volume fractions and initial gas and liquid velocities and liquid head on the tray deck have been set for different zones. Empirical correlations exist for predicting steady state values of these parameters in different zones [23]. When steady state condition for sieve tray is governed, packed zone equations should be added to the domain. In the simulation procedure, steady condition is assumed as a condition in which clear liquid height does not change significantly with time while the program is running. To improve convergence conditions, at the start of the simulation of PST, only Ergun source terms are taken into account for the packed zone fol-

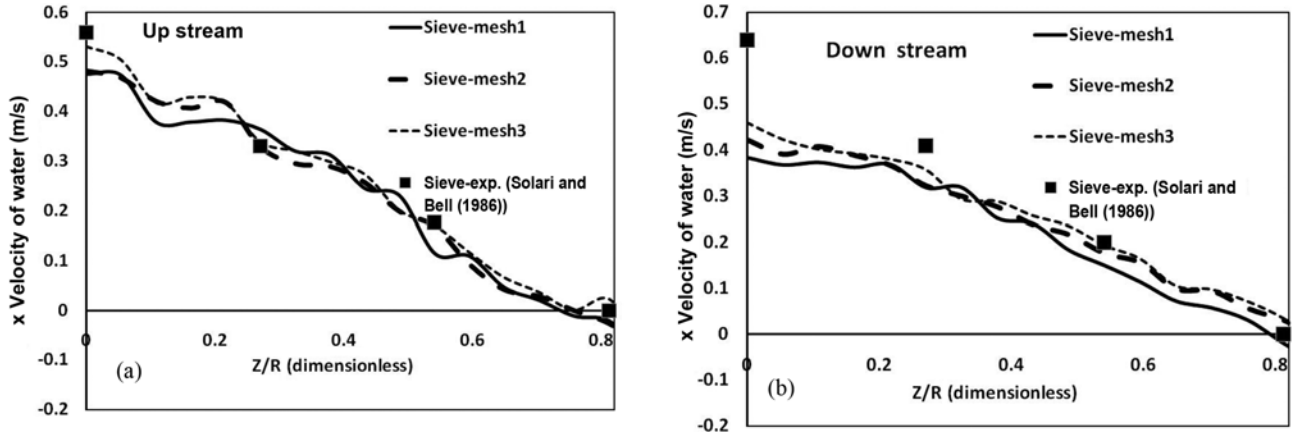

Fig. 3. Mesh independency analysis in sieve tray (a) Upstream position of tray (b) Downstream position of tray at F_s=0.462 ($kg^{0.5}\cdot m^{-1}\cdot s^{-0.5}$) and Q=17.8*10^{-3} ($m^3s^{-1}$).

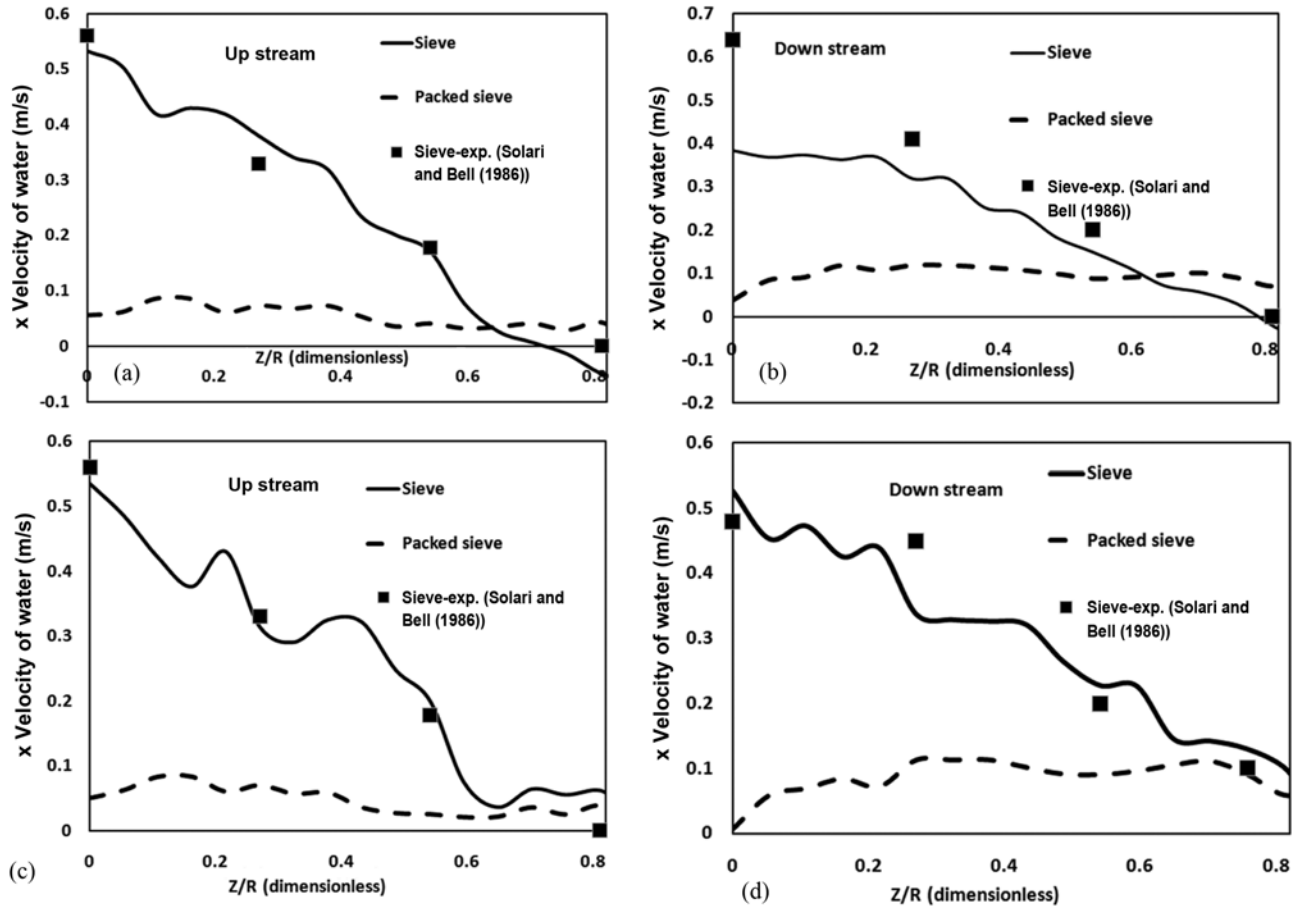

Fig. 4. Velocity distribution in sieve and packed sieve trays with experimental data of sieve tray (a) Upstream (b) Downstream at the operating conditions of F_s=0.462 ($kg^{0.5}\cdot m^{-1}\cdot s^{-0.5}$) and Q=17.8*10^{-3} ($m^3s^{-1}$) at the height of the 0.038 m from tray floor, and (c) Upstream and (d) Downstream at the operating conditions of F_s=0.801 ($kg^{0.5}\cdot m^{-1}\cdot s^{-0.5}$) and Q=17.8*10^{-3} ($m^3s^{-1}$) at the height of 0.038 m from the tray deck.

lowed by the inclusion of drag force term developed for this zone (Eqs. (8) and (13)). After that, clear liquid height is monitored again to reach a constant value as an indicator for the steady state condition. SIMPLE algorithm with upwind differencing method was used to solve the equations. Time increment is used in the simulation in the range of 0.005 to 0.0005 seconds. To reach rapid convergence, at the initial steps of simulation, usually the time increment value is considered as a small value such as 0.0005, and after enough time, this value enhanced to larger values of about 0.005. At the end, program running is continued until reaching steady state condition by considering all relevant presented equations. Simulations have been done on Intel® xenon (CPU) 2.33 GHz-2 processors run in parallel form.

RESULTS AND DISCUSSION

The CFD analysis and simulations were performed by using the commercial package FLUENT6.3.26. In this section simulation results are presented. Initially, sieve tray simulations were performed. Having achieved close agreement between model and experimental results for sieve tray, we added packing. Simulations were run at different gas and liquid velocities and the results were compared with the sieve tray results. At the initial step, it is required to study the mesh independency.

1. Mesh Independency

Experiment data of Solari and Bell [24] have been used to validate the current study. Simulated sieve tray dimensions are based on tray properties of Solari and Bell [24] experimental works shown in Table 1 ini the manuscript. The geometry of tray layout is shown in Fig. 2(b) with the probe layout shown by numbered positions. Probe positions were located about 0.038 m from tray floor. Solari and Bell calculated the average liquid velocity values by dividing the distance between two consecutive probes located in the same longitudinal row by the difference in mean residence time between two probes. Referring to Fig. 2(b), they measured the velocities along the probe line composed of (8-12), (7-11), (6-10) and (5-9) lines and called as upstream x-velocity of water at the upstream (middle section of tray). In the same way, velocity values were measured along the probe line composed of (12-16), (11-15), (10-14) and (9-13) lines and called as x-velocity of water at the downstream (tray outlet).

To compare between CFD simulation results with experimental data, average of water x-velocity was calculated on the plane of y= 0.038 m between the x=0.209 m and x=0.438 (Fig. 2). The values were calculated based on the Eq. (21) along every line, located between x=0.209 and x=0.438. These lines are observable in Fig. 2. Resulting profiles have been selected as upstream profiles. In the same way, calculations were performed on the lines between x=0.438 and x=0.667 on the plane y=0.038 (middle of the tray and outlet weir). Resulting profiles are referred to as downstream profiles [12].

$$u_{ave} = \frac{\int u dx}{l} \tag{21}$$

Where;

u_{ave} is the X-component of linear average of water velocity along with every lines in upstream and downstream sections in Fig. 2(b) and l is the line length. Referring to Fig. 3 and 4, these values have been illustrated with the almost continuous curves and experimental values are shown with discontinuous points, noting that the X-coordinate is dimensionless values of X-values along the tray deck.

Mesh independency means that after certain mesh size, the results do not change considerably when the mesh density is increased. Three different mesh densities were used in the present work. Mesh1 has 28306 cells and mesh2 and mesh3 have 74498 and 156200 cells, respectively. The grid system for this model is complicated, so Tet/Hybrid elements with TGrid mesh types have been used. Referring to Fig. 3(a) and (b), there is no considerable change in the mesh2 and mesh3 velocity profiles, so mesh2 has been used in the simulations.

It is worthy to note that, small numbers of the holes (45 holes on one half of the tray) were considered in order to prevent more computational time. Small numbers of the holes require low mesh densities, so, computational time is decreased.

As can be seen from Figs. 3(a) and 3(b), there is close agreement between sieve tray model results and experimental data.

2. Velocity Distribution in Sieve Trays and PSTs

Water horizontal velocity for the sieve and PSTs is demonstrated

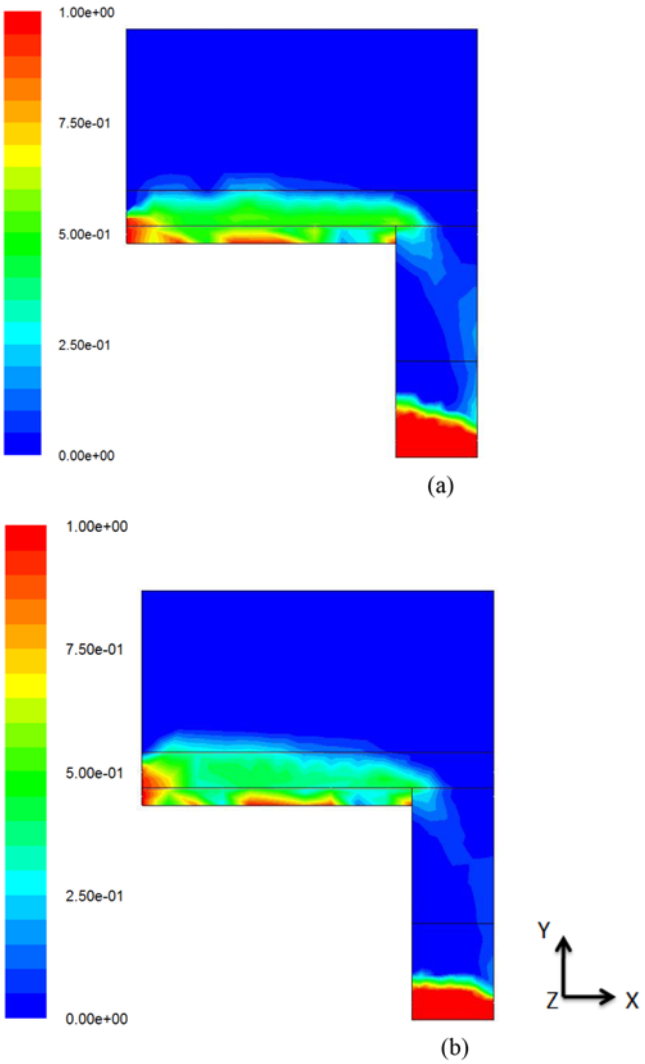

Fig. 5. Liquid volume fraction contours at the (a) sieve and (b) Packed sieve tray at the operating conditions of Q_l=17.8* 10^{-3} (m^3s^{-1}), F_s=0.801 ($kg^{0.5}\cdot m^{-0.1}\cdot s^{-0.5}$) on the XY plane.

in Fig. 4. Experimental data of sieve tray [24] are also presented in these graphs. The water velocity tends to decrease from tray center (z/R=0) to the walls. This trend is confirmed by the experimental results. Different operational conditions (especially changes in gas flow rate) have a dominant effect on the liquid velocity distribution in the sieve tray that was also mentioned by Solari and Bell [24]. The slight oscillations observed in Figs. 4(c) and 4(d) are also caused by higher gas rate rising through a small number of the holes. Reduction in circulation area adjacent the wall section of tray (points with the velocity lower than 0.1 at Fig. 4) is also observable in Fig. 4(d) with respect to Fig. 4(b) in the sieve tray. This is caused by small increase in gas velocity.

There is a difference between the simulated and experimental data in Fig. 4(b). These errors have also been observed in the previous works (please see ref. 15, Figs. 2(b) and 3(b) and ref. 12 Figs. 4, 6 and 7). Certain grid resolution near the walls can reduce the error sources. But errors are not disappeared completely. K-ε turbulence method and Eulerian-Eulerian multiphase model with specified drag coefficient has been used in the present study. Empirical Bennett et al. correlation [11], used in drag coefficient (Eq. (9)), causes some errors in the volume fraction predictions and consequently in the velocity results. Using more expensive computational cost LES method with VOF multiphase model may give better results due to more precise evaluation of specified shear and wall functions with respect to the k-ε method in the three dimensional flows (please see ref. 14 Fig. 8). VOF method does not include any drag coefficient because of its formulation method.

The water velocity remains almost constant in the z-direction at every point of the tray deck in the case of PST. It means that the addition of packing results in velocity uniformity in the tray due to the viscous and inertial losses. In the case of using sieve tray, there are stagnant regions near the tray walls, appearing as low velocity points at the end of all upstream and downstream graphs (Figs. 4(a)-(d)). These points almost disappeared on PST as packing acts as a deflector near the walls.

3. Water Volume Fraction Contours at XY Plane

Figs. 5(a) and 5(b) demonstrate water volume fraction contours in a symmetric plane on sieve and PSTs. Increase of froth height is remarkable in the presence of packing on the PST. Inertial and viscous losses in the packed zone cause losses in dynamic pressure of both liquid and gas phases, so they accumulate on the tray and result in an increase in the froth height. Consequently, packing can result in improving separation and residence time and lead to higher tray efficiency.

Solid volume is not clearly seen in the equations, but its effect has been indirectly considered by pressure drop terms in the momen-

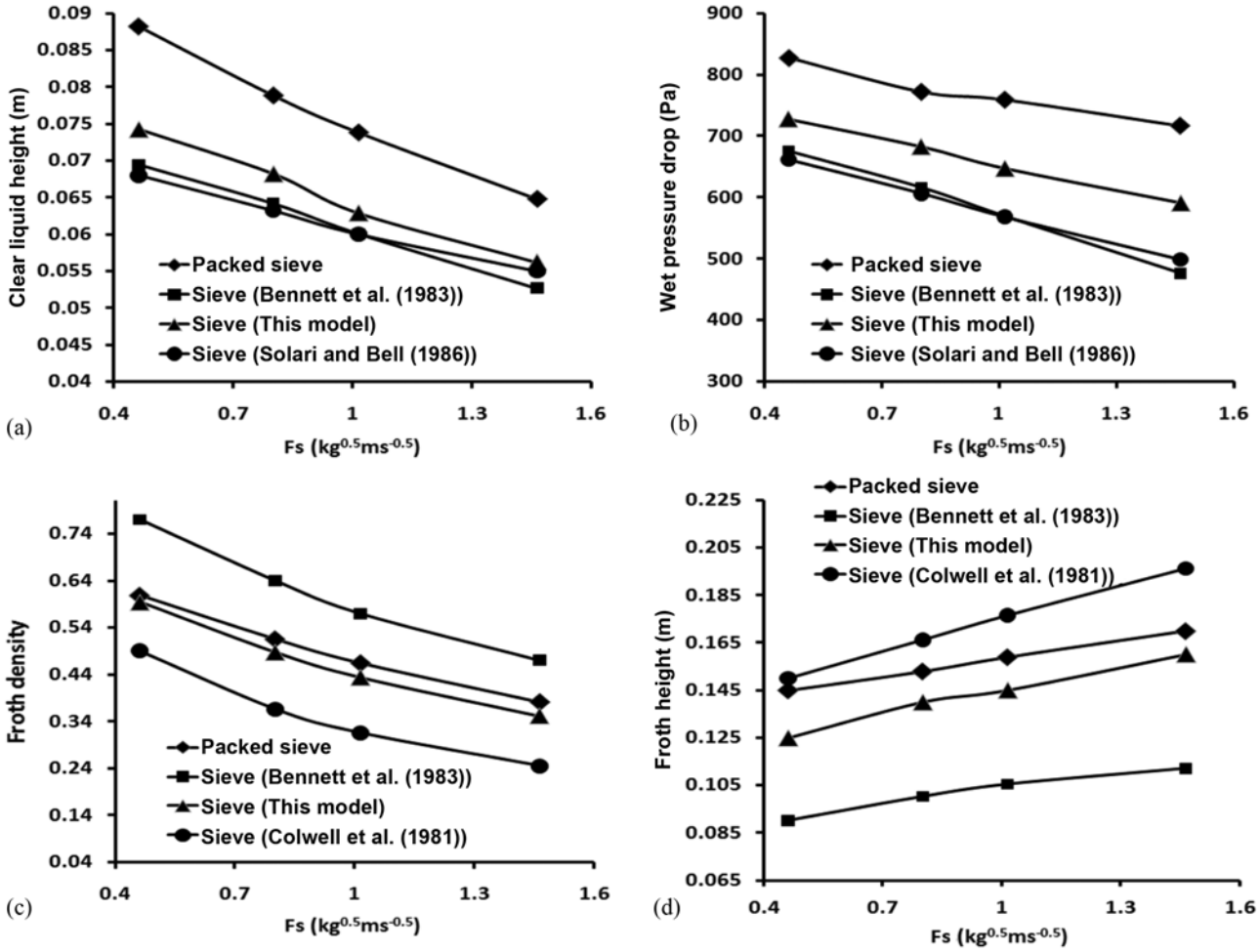

Fig. 6. Hydraulic parameters of sieve and packed sieve tray at the different gas superficial velocities and liquid flow rate of Q=17.8*10^{-3} (m^3s^{-1}) (a) Clear liquid height, (b) Wet pressure drop, (c) Froth density, (d) Froth height.

tum equations and consequently in the velocity terms (terms F_{GS} and F_{LS} at the Eq. (3) and (4)). Gas phase residence time is improved in the tray due to pressure losses in the presence of packing. Consequently, gas volume fraction in the heights near the tray floor increases. The more gas in the packed zone, the more space is occupied by gas phase and liquid phase sits on the higher elevations and froth height increases.

4. Hydraulic Parameters and Wet Pressure Drop of PST

The clear liquid height can be accurately determined on sieve trays by integrating vertical liquid holdup profiles [23]. Therefore, it has been calculated in the following way:

$$hl = \int \alpha_{ave,y} dy = \int \frac{\iint \alpha \, dx dz}{A} dy = \frac{\iiint \alpha dx dz dy}{A} = \frac{\int \alpha dv}{A} \quad (22)$$

Where, $\alpha_{ave,y}$ is the surface average of the water volume fraction on the surfaces located in parallel direction with respect to the tray deck at the given y. These surfaces have constant area that equals the tray deck surface area. The last term in the Eq. (22) can be calculated numerically to get clear liquid height.

Froth region is the region in which water volume fraction is larger than 10% [23]. So, the average of froth height is the height from the tray floor, at which the average of water volume fraction starts to fall below 10 percent. X-Z planes were considered parallel to the tray floor at the different height. The height that the average of water volume fraction is less than 10% will be considered as froth height. Froth density is calculated as the ratio of clear liquid height to the froth height [23].

Fig. 6 illustrates that the prediction of clear liquid height on sieve tray is in good agreement with Bennett et al.'s correlation [11]. Generally, at different air velocities, clear liquid height is larger for PST. As indicated in Fig. 6(a), clear liquid height is almost 17 percent greater in PST. Chen et al. [2] reported that this is due to smaller bubble size and more stable conditions. There is an overprediction in the estimation of clear height with CFD modeling. The reason is that the interaction term of Eq. (9) is not exact due to the model as-

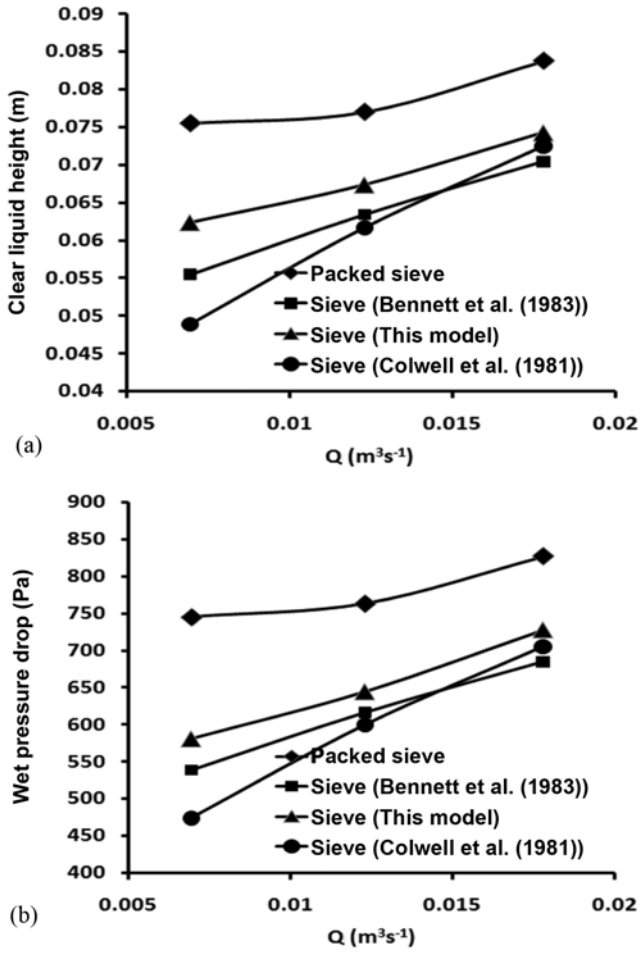

Fig. 7. Effect of liquid flow rate on the (a) Clear liquid height (b) Wet pressure drop of sieve and packed sieve trays at constant gas F-factor F_s=0.462 ($kg^{0.5}\cdot m^{-0.1}\cdot s^{-0.5}$).

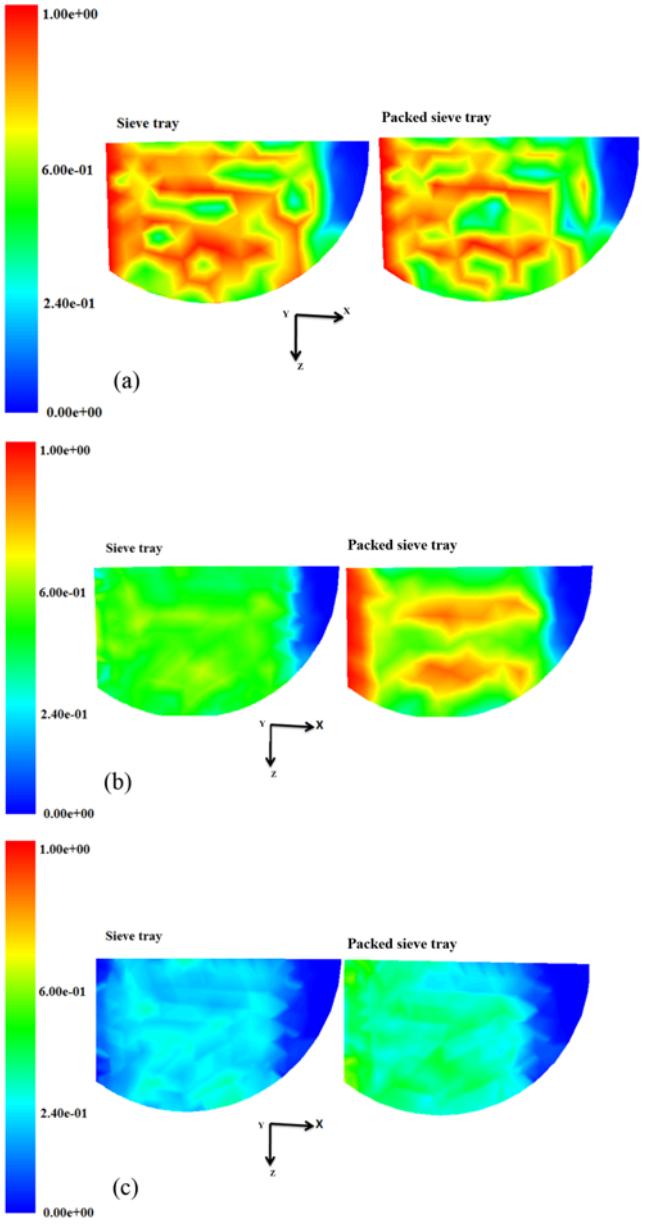

Fig. 8. Water volume fraction contours in XZ plane at different elevations at the operational conditions of F_s=0.801 ($kg^{0.5}\cdot m^{-1}\cdot s^{-0.5}$), Q=17.8*$10^{-3}$ at the different heights of tray floor, (a) 0.025 m, (b) 0.042, (c) 0.06 m.

sumptions [12].

Clear liquid height has an important role in the static and total pressure values, so that increasing of clear liquid height is a reason for additional pressure drop in PST (Fig. 6(b)). Wet pressure drop graphs follow the same trend as clear liquid height.

There is good agreement between the CFD results and the momentum balance equation based on Bennett et al. [11] (Eq. (22)) or Colwell [13] (Eq. (15)) correlation. PST wet pressure drop is obviously higher than sieve tray at any gas superficial velocity. Simulation results showed that this increasing is about 16 percent. Chen et al. [2] reported this value as being about 10 to 20 percent in the air-water system based on their experimental observations.

Due to more liquid accumulation on the tray deck, froth density and froth height are moderately higher for PSTs compared to sieve tray. Simulation results show that packing increases froth density up to 6 and froth height to the 10 percent.

Effect of change in liquid flow rate on the clear liquid height and wet pressure drop of sieve and PSTs and their comparison with sieve tray correlations is demonstrated in Fig. 7. Increasing liquid flow rate causes an increase in clear liquid height and consequently wet pressure drop, due to the lower liquid and gas interactions at higher liquid flow rates. According to the simulation results, clear liquid height and wet pressure drop are relatively larger for PST compared to sieve tray at any given liquid flow rate as shown in Fig. 7.

5. The Liquid Volume Fraction Distribution

Fig. 8 illustrates liquid volume fraction contours. This figure demonstrates and compares the liquid distribution pattern in the mixture at different elevations for both sieve and PSTs. At lower heights, inside the packed zone (Fig. 8(a)), there is a tendency for accumulation of more gas inside the mixture. Therefore, more gas exists at lower elevations in PSTs, causing more interaction between two phases, which could result in higher tray efficiency.

Above the packing section, the mixture tends to have more liquid volume fraction due to liquid finding not much opportunity to fill

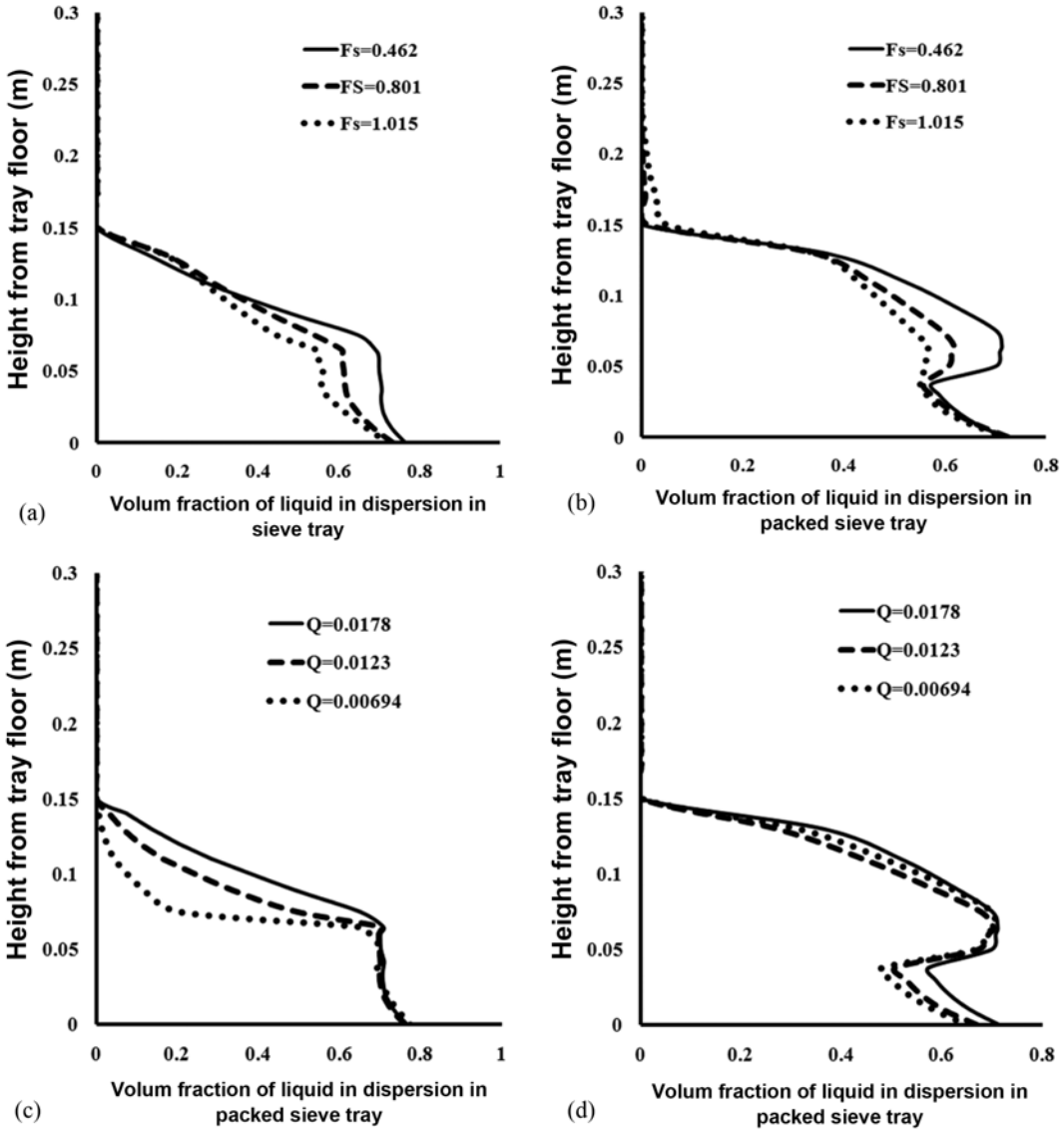

Fig. 9. Effect of operational conditions on liquid and gas volume fraction distribution at the XZ plane at different height and operating conditions of Q=17.8*10^{-3} (m^3s^{-1}) and different gas velocities at the (a) sieve (b) packed sieve tray and at the F_s=0.801 ($kg^{0.5}\cdot m^{-1}\cdot s^{-0.5}$) and different liquid flow rates at the (c) sieve, (d) packed sieve tray.

the packed zone already filled with gas. Therefore, in case of PST there is a considerable liquid volume fraction at a height of 0.06 m from the tray deck (Fig. 8(c)). These figures obviously describe differences in liquid and gas flow pattern on the tray deck.

Liquid volume fraction distributions at different heights from tray deck are shown in Fig. 9(a)-9(d). To report these data, parallel plates with respect to the tray deck have been considered. The average of water volume fraction has been calculated from Eq. (23) at the given y on every specified plane. Resulting graphs are specified in Fig. 9.

$$\alpha_{ave,y}=\left(\frac{\int\alpha dA}{\int dA}\right)_y=\left(\frac{\int\alpha dA}{A}\right)_y \quad (23)$$

Where $\alpha_{ave,y}$ is the average of water volume fraction at the given height y.

At heights lower than the weir height, there is almost uniform mixture with higher volume fraction of water for sieve tray (vertical lines in sieve tray curves in Fig. 9(a)). With increases in F-factor, these vertical lines shifted to slightly smaller volume fraction values on the water volume fraction axis. These behaviors have also been reported by other authors [21,23].

Like water volume distribution on sieve tray, several simulations have been done to predict these graphs for PST (Fig. 9(b)). Gas phase accumulation is initially larger in packed zone, so vertical lines in the sieve tray graphs are the lines with smaller slope in the PST graphs. Above the packed zone, liquid volume fraction extends to larger values stretching up to the weir height. At the same height from the tray deck, in the froth region, the packed tray has larger value of water volume than sieve tray. So accumulation of more liquid is also observable in this graph. Liquid flow rate variation effects on the water volume distribution are shown in Fig. 9(c) and (d).

CONCLUSIONS

Packed sieve tray properties have been studied. Properties such as velocity distribution, clear liquid height, froth height and density and phase volume fraction distribution at different elevations from the tray deck and wet pressure drop have been investigated on PST and compared to similar ones in the sieve tray. For this reason, initially sieve tray is modeled as three-dimensional two-phase flow of air and water in Eulerian-Eulerian frame work. By defining the slice thickness of the tray deck as packed zone, PST geometry has been created. It is concluded from the results that the presence of packing causes an approximate increase in clear liquid height, froth density, froth height and wet pressure drop by 17, 6, 10 and 16 percent, respectively. Therefore, it improves conventional sieve tray characteristics.

ACKNOWLEDGEMENT

The authors are grateful for financial support from the Azar Energy Company.

NOMENCLATURE

A : plane surface parallel to the tray floor [m^2]
A_{hole} : total area of the holes [m^2]
A_b : tray bubbling area [m^2]
a_{ave} : average of water volume fraction at the planes parallel to the tray deck [-]
$a_{y,ave}$: average of water volume fraction at the given height [-]
a_p : specific surface area [m^2/m^3]
C_D : drag coefficient [-]
d_G : bubble diameter [m]
F_S : F factor= $V_s\sqrt{\rho_G}$ [$(kg/m)^{0.5}\ s^{-1}$]
F_{GS} : momentum source term due to porous zone in the gas momentum equation [N/m^3]
F_{LS} : momentum source term due to porous zone in the liquid momentum equation [N/m^3]
g : gravity acceleration [m/s^2]
h_{ap} : clearance under downcomer [m]
h_f : froth height [m]
h_l : clear liquid height [m]
h_w : weir height [m]
h_{ow} : liquid height above weir height [m]
$M_{G,L}$: inter phase momentum transfer [N/m^3]
n : total number of the holes
P : pressure [N/m^3]
Q : liquid volumetric flow rate [m^3/s]
t : time [s]
U : velocity vector [m/s]
u : x-component of velocity [m/s]
v : y-component of velocity [m/s]
w : z-component of velocity [m/s]
u_l : liquid-phase superficial velocity [m/s]
u_{ave} : x-component of water average velocity [m/s]
V_h : gas hole velocity [m/s]
V_{slip} : slip velocity [m/s]
V_s : gas-phase superficial velocity based on bubbling area [m/s]
W : weir length [m]

Greeks

α_G : gas holdup fraction [-]
α_L : liquid holdup fraction [-]
$\alpha_{G,Ave}$: average gas holdup fraction in froth [-]
$\alpha_{L,ave}$: average liquid holdup fraction in froth [-]
$\alpha_{G,Ave}^*$: modified Average gas holdup fraction in porous zone [-]
$\alpha_{L,Ave}^P$: average liquid holdup fraction in porous zone [-]
$\alpha_{ave,y}$: average of the water volume fraction on the surfaces [-]
φ : hole area ratio to the bubbling area [-]
μ : dynamic viscosity [$kg\cdot m^{-1}\cdot s^{-1}$]
ρ : density [kg/m^3]
ε_p : porosity [-]

Subscripts

eff : effective
G : gas phase
L : liquid phase

REFERENCES

1. D. A. Spagnoloand and K. T. Chuang, *Ind. Eng. Chem. Pro. Des. Dev.*, **23**, 561 (1984).
2. G X. Chen, A. Afacan, C. Xu and K. T. Chuang, *Can. J. Chem. Eng.*, **68**, 382 (1990).

3. G. X. Chen, K. T. Chuang, C. Chien and Y. Ye, *Gas Sep. Pur.*, **6**, 207 (1992).
4. G. X. Chen, *Predicting and improving sieve tray efficiency sieve tray efficiencies in distillation*, Ph. Thesis, University of Alberta (1993).
5. Abu Bakr S. H. Salem, *Sep. Sci. Technol.*, **28**, 2255 (1993).
6. B. Mehta, K. T. Chuang and K. Nandakumar, *Chem. Eng. Res. Des.*, **76**, 834 (1998).
7. B. Mehta, *Model for liquid phase flow on sieve trays*, Msc. Thesis, University of Alberta (1997).
8. C. H. Fischer and J. L. Quarini, *Three-dimensional heterogeneous modeling of distillation tray hydraulics*, AIChE Meeting, Miami Beach, USA (1998).
9. C. J. Liu, X. G. Yuan, K. T. Yu and X. J. Zhu, *Chem. Eng. Sci.*, **55**, 2287 (2000).
10. J. M. Van Baten and R. Krishna, *Chem. Eng.*, **77**, 143 (2000).
11. D. L. Bennett, R. Agrawal and P. J. Cook, *AIChE J.*, **29**, 434 (1983).
12. G. K. Gesit, K. Nandakumar and K. T. Chuang, *AIChE J.*, **49**, 910 (2003).
13. C. J. Colwell, *Ind. Eng. Chem. Pro. Des. Dev.*, **20**, 298 (1981).
14. J. G. Teleken, L. O. Werle, I. G. B. Parisotto, C. Marangoni, A. P. Meneguelo, Ricardo and A. F. Machado, *Fluid-dynamics study of multiphase flow in a sieve tray of a distillation column*, 20th European Symposium on Compute Aided Process Engineering-ESCAPE20 (2010).
15. T. Zarei, R. Rahim and M. Zidvar, *Korean J. Chem. Eng.*, **26**, 1213 (2009).
16. A. Alizadehdakhel, M. Rahimi and A. Abdulaziz Alsairafi, *Korean J. Chem. Eng.*, **26**, 475 (2009).
17. X. Gang Li, D. Xin Liu, Sh. Min Xu and H. Li, *Chem. Eng. Process.*, **48**, 145 (2009).
18. Z. Olujic, M. Jodecke, A. Shilkin, G. Schuchb and B. Kaibel, *Chem. Eng. Process.*, **48**, 1089 (2009).
19. R. Rahimi and D. Abbaspour, *Chem. Eng. Process.*, **47**, 1504 (2008).
20. F. Yin, *Liquid maldistribution and mass transfer efficiency in randomly packed distillation column*, Ph. Thesis, University of Alberta (1999).
21. H. Z. Kister, Distillation Design, McGraw-Hill, New York (1992).
22. F. Yin, Z. Wang, A. Afacan, K. Nandakumar and K. T. Chuang, *Can. J. Chem. Eng.*, **78**, 449 (2000).
23. M. J. Lockett, Distillation tray fundamental, Cambridge University Press, Cambridge (1968).
24. B. Solari and R. L. Bell, *AIChE J.*, **32**, 640 (1986).
25. J. P. Kachur, A. Afacan and K. T. Chuang, *Chem. Eng. Res. Des.*, **82**, 813 (2004).